tvst

Article

Retinal Microvascular Alterations Detected by Optical Coherence Tomography Angiography in Nonfunctioning Pituitary Adenomas

Xuqian Wang[1–4,*], Yuyu Chou[1–3,*], Huijuan Zhu[3–5], Bing Xing[3–6], Yong Yao[3–6], Lin Lu[3–5], Hui You[3,4,7], Linyang Gan[1,2], Meng Wang[1,2], Jin Ma[1–4], and Yong Zhong[1–4]

[1] Department of Ophthalmology, Peking Union Medical College Hospital, Chinese Academy of Medical Sciences & Peking Union Medical College, Beijing, P. R. China
[2] Key Laboratory of Ocular Fundus Diseases, Chinese Academy of Medical Sciences, Beijing, P. R. China
[3] China Pituitary Disease Registry Center, Beijing, P. R. China
[4] China Pituitary Adenoma Specialist Council, Beijing, P. R. China
[5] Key Laboratory of Endocrinology of Ministry of Health, Peking Union Medical College Hospital, Chinese Academy of Medical Sciences and Peking Union Medical College, Beijing, P. R. China
[6] Department of Neurosurgery, Peking Union Medical College Hospital, Chinese Academy of Medical Sciences and Peking Union Medical College, Beijing, P. R. China
[7] Department of Radiology, Peking Union Medical College Hospital, Chinese Academy of Medical Sciences and Peking Union Medical College, Beijing P. R. China

Correspondence: Yong Zhong. e-mail: zhongy_pumch@126.com
Jin Ma. e-mail: majin1912@163.com

Received: September 8, 2021
Accepted: December 10, 2021
Published: January 5, 2022

Keywords: vessel density; microvascular alteration; nonfunctioning pituitary adenomas; optical coherence tomography angiography

Citation: Wang X, Chou Y, Zhu H, Xing B, Yao Y, Lu L, You H, Gan L, Wang M, Ma J, Zhong Y. Retinal microvascular alterations detected by optical coherence tomography angiography in nonfunctioning pituitary adenomas. Transl Vis Sci Technol. 2022;11(1):5, https://doi.org/10.1167/tvst.11.1.5

Purpose: Visual impairment assessment plays a significant role in diagnosis and clinical decisions in nonfunctioning pituitary adenoma (NFPA). Retinal microvascular alterations may potentially reflect the visual impairment. The purpose of this study was to evaluate fundus microvascular alterations in patients with NFPA.

Methods: Comparisons of visual field, retinal structure, and microcirculation were conducted between patients with NFPA and age- and sex-matched healthy controls. Multivariate regression modeling was used to assess the relationship between symptom duration, sellar mass size, and fundus vessel density (VD) of patients. Receiver operating characteristic (ROC) curves were depicted to determine the diagnostic performance of significant parameters to discriminate eyes with NFPA from healthy eyes.

Results: Forty eyes of patients and 40 eyes of healthy individuals were enrolled. Compared to healthy controls, patients with NFPA had a larger foveal avascular zone area and thinner ganglion cell complex thickness. The VDs of patients presented an obvious decrease in radial peripapillary capillary (RPC) and an increase in the deep capillary plexus segment of the perifoveal area. The peripapillary VDs of patients were significantly related to sellar mass size. The area under the ROC curve of VD in the RPC segment of the temporo-inferior sector was the largest (0.801; 95% confidence interval, 0.70–0.90; $P < 0.001$).

Conclusions: The fundus of patients with NFPA demonstrated significant and characteristic microvascular impairments. The VDs were also significantly associated with sellar mass size.

Translational Relevance: Retinal microvascular alterations detected by optical coherence tomography angiography are characteristic and related to sellar mass size, which may provide information that facilitates the diagnosis of NFPA.

Introduction

As one of the most common types of pituitary adenomas (PAs), nonfunctioning pituitary adenomas (NFPAs) have a prevalence of 7 to 41.3 per 100,000 people, and their incidence rate is 0.65 to 2.34/100,000.[1] As described, NFPAs are characterized by a lack of hormone-related clinical symptoms and signs.[2] This absence of indications creates several difficulties in the early diagnosis of NFPA. Visual symptoms, including vision loss and visual field defects (VFDs), can be observed in approximately 60% of patients with NFPA.[3,4] Notably, the extent of visual impairment also plays a significant role in clinical decisions regarding aspects of the optimal therapeutic strategy, such as the accurate timing of surgery.[5] Supporting this notion, ophthalmic examinations of patients with NFPA are considerably important for disease diagnosis and surgery decisions.

Among several ancillary ophthalmic examinations, perimetry and visual evoked potential have been shown to enable the identification of an impaired visual field (VF) or visual pathway. However, these examinations only evaluate functional visual damage that has already happened, and the results of the two examinations are relatively subjective and time-consuming. Concerning these limitations, many studies have been conducted to explore more convenient, objective, and quantitative measurements for evaluating patients with visual impairments who have NFPAs.

Based on the theory that retinal ganglion cells (RGCs) are sensitive to hemodynamic changes[6] and retinal microcirculation attenuation may be secondary to RGC axonal retrograde degeneration or directly induced by chiasmal compression, a few studies have explored the fundus vessel densities (VDs) of patients with PA by using optical coherence tomography angiography (OCTA). OCTA is a high-speed, quantitatively measured, and noninvasive fundus blood flow mapping method. Recently, it has been demonstrated that the blood flow of the superficial capillary plexus (SCP) decreases in patients with PAs,[7,8] but the changes in perfusion of the deep capillary plexus (DCP) from different studies are inconsistent.[9,10] Additionally, those studies were conducted among patients with different types of PA or sellar mass lesions, which did not allow a distinction between the potential effects of abnormal hormone secretion and local mass effects on fundus microvascular changes.

To avoid the potential effect of abnormally secreted hormones on fundus microcirculation, we evaluated retinal microvascular alterations only in patients with NFPA using OCTA. Considering the characteristic impairment of retinal structure caused by the sellar mass effect, our study also assessed VDs in different subsectors to explore whether the changes in microcirculation were consistent with the structural alterations. A comparison of diagnosis abilities was conducted among the parameters of VDs, visual function, and retinal structure.

Methods

This was a retrospective, cross-sectional, and observational study in accordance with the tenets of the Declaration of Helsinki. Its protocol was approved by the Institutional Review Board of Peking Union Medical College Hospital, Chinese Academy of Medical Sciences. Due to the retrospective nature of this study, patient consent was waived (ethics approval number: S-k1390).

Study Design and Participants

In this study, we comprehensively reviewed patients with naive NFPA and age- and sex-matched healthy controls between January 2019 and April 2020 at Peking Union Medical College Hospital (PUMCH) in China. Some of these participants were also included in another study at the same department, but the data were not duplicated. The medical records of all participants before surgery were extracted. The extracted data included demographic information, chief complaint, self-reported disease duration from symptom onset to diagnosis of tumors, ophthalmic test, pituitary magnetic resonance imaging (MRI) outcomes, and results of other systemic tests.

Patients who met the diagnostic criteria of NFPA according to the World Health Organization classification[11] were enrolled in this study. Only a single eye with worse VFD was included in the analysis. Healthy control individuals were colleagues who worked at PUMCH and had no obvious abnormalities in craniocerebral computed tomography scans and fundus examinations, according to the results of their annual routine physical examinations. Exclusion criteria for patients and healthy individuals were as follows: (1) participants having been treated with pituitary or ocular surgery, radiotherapy, or endocrine therapy; (2) participants with abnormal hormone secretion or systemic diseases that might affect retinal structure and VD, such as diabetes and uncontrolled hypertension; (3) participants with another ophthalmic comorbidity affecting retinal microcirculation or structure such as age-related macular degeneration, retinal vein

occlusion, and glaucoma; (4) participants with ocular diseases that affect the imaging quality of OCTA or optical coherence tomography (OCT), such as severe cataract or vitreous opacity; (5) spherical equivalents (SEs) smaller than –6.0 diopters (D), indicating high myopia, or greater than +3.0 D, indicating moderate hyperopia; and (6) other sellar mass lesions such as meningioma and craniopharyngioma.

Suprasellar Extension Measurement

MRI scans were measured for suprasellar extension (SSE)[12] in both sagittal and coronal images. They were conducted independently by J.M. and Y.C., who were masked to other clinical records. Coronal SSE was measured from the highest point of the tumor to the level of the bilateral internal carotid artery's upper surfaces, while sagittal SSE was considered the distance from the line drawn between the tuberculum and dorsum sellae to the highest point of tumor.

Ocular Examinations

All patients and healthy controls underwent examinations that included the best corrected visual acuity (BCVA) presented as the logarithm of the minimum angle of resolution, SE, intraocular pressure (IOP), comprehensive slit-lamp examination, static VF examination, and OCT/OCTA scanning. Static automated perimetry was performed with the Octopus 900 perimeter (Haag-Streit, Köniz, Switzerland) after correcting refractive errors, if any. The tendency-oriented perimetry was adopted. VFDs were quantitatively assessed by mean deviation (MD) and mean sensitivity. Reliability criteria were defined as reliable factor <14%.

Fundus microvascular and structural changes were obtained by Angiovue RTVue XR Avanti (Optovue, Inc, Fremont, CA, USA). All participants underwent angio retina mode (high definition (HD) 6 × 6 mm centered on the fovea), angio disc mode (HD 4.5 × 4.5 mm centered on optic disc), ganglion cell complex (GCC) mode, and optic never head mode scanning. Only high-quality scans (those with a quality index [QI] ≥7/10) were eligible for analysis. AngioVue software automatically calculated VDs with a projection-resolved algorithm, foveal avascular zone (FAZ) metrics, and retinal thickness parameters in different sectors and retinal layers.

The different layers and sectors measured in OCT scans were determined automatically. Reliability criteria were defined as both false-positive and false-negative rates as follows: (1) VD was regarded as the area ratio of microvascular density. (2) Radial peripapillary capillary (RPC) was detected in the layer from the internal limiting membrane (ILM) to the nerve fiber layer posterior boundary. (3) The SCP was the segment from the ILM to 9 mm above the junction between the inner plexiform layer (IPL) and the inner nuclear layer (INL). (4) The DCP was the segment from 9 mm above the IPL–INL junction to the junction between the outer plexiform layer and outer nuclear layer. (5) Angio disc scans were divided into eight subsectors (nasal-superior; nasal-inferior; inferior-nasal, IN; inferior-temporal, IT; temporo-inferior, TI; temporo-superior; superior-temporal, ST; and superior-nasal, SN) based on the Garway Heath method. (6) The measured area of peripapillary retinal nerve fiber layer (pRNFL) thickness was automatically and evenly divided into eight subsectors: nasal-upper, nasal-lower, IN, IT, temporo-lower, temporo-upper, ST, and SN sectors. (7) Angio retina scans were automatically divided into four quadrants (superior, temporal, inferior, and nasal) according to the fovea-centered Early Treatment Diabetic Retinopathy Study (ETDRS) grid, whereas the GCC mode only provided superior and inferior hemispheres. (8) In accordance with the ETDRS grid, the foveal zone was the area within the smallest circle with a diameter of 1 mm centered macula, and the parafoveal zone was the annular region between two circles with diameters of 1 mm and 3 mm. The perifoveal zone was the annular region between two circles with diameters of 3 mm and 6 mm (Fig. 1).

Statistical Analysis

All statistical analyses were conducted using SPSS software (SPSS for Mac, version 23.0; IBM/SPSS, Chicago, IL, USA). Categorical and continuous variables are presented as frequencies (or percentages) and means ± standard deviations (SDs), respectively. Normality was confirmed by inspecting histograms and by the outcomes of the Shapiro–Wilk test. To compare the differences between the NFPA group and the control group, independent sample *t*-tests and Mann–Whitney tests were assessed for normally distributed variables and nonnormal variables, respectively. Linear regression analysis was conducted after adjusting for age, sex, SE, and QI to further confirm the differences in VDs between patients and healthy controls. Multivariate regression modeling was used to assess the relationship between VD and visual function, retinal structure, and tumor size when adjusting for age, sex, SE, and QI. Receiver operating characteristic (ROC) curves were depicted to determine the diagnostic performance of significant measurements to discriminate eyes with NFPA from control eyes. The area under the ROC curve (AUC) values were

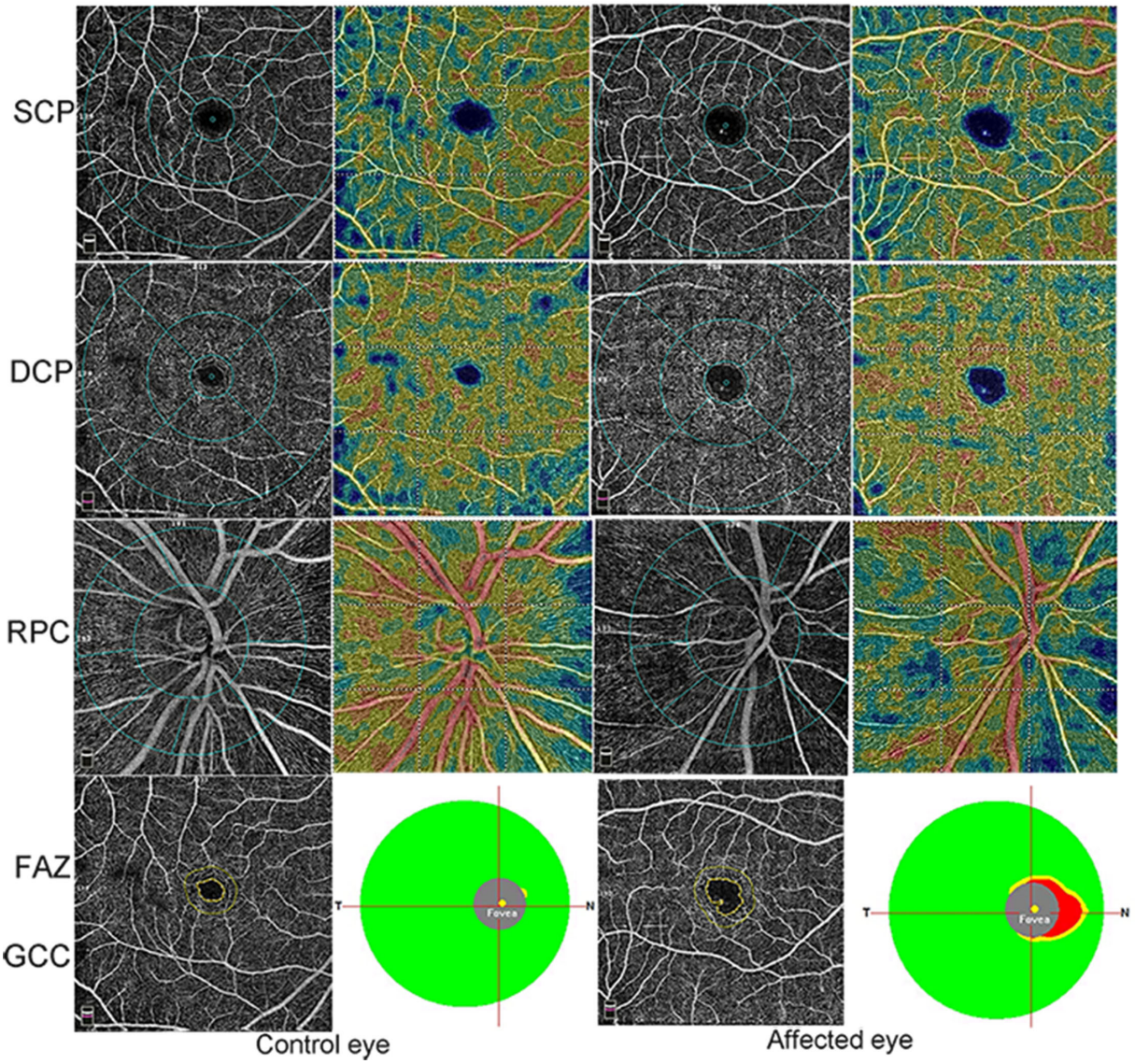

Figure 1. Comparisons of vessel density, foveal avascular zone measurements, and ganglion cell complex thickness between healthy control eyes (two left columns) and eyes with NFPA (two right columns). Retinal scans were automatically divided into four quadrants as superior (S), temporal (T), inferior (I), and nasal (N) according to the fovea-centered ETDRS grid. Disc scans were divided into eight subsectors (nasal-superior, NS; nasal-inferior, NI; inferior-nasal, IN; inferior-temporal, IT; temporo-inferior, TI; temporo-superior, TS; superior-temporal, ST; and superior-nasal, SN) based on the Garway Heath method.

recorded. When the Youden index (sensitivity + specificity – 1) was maximized, the optimal cutoff value and the corresponding sensitivity and specificity were also determined. P values <0.05 were considered statistically significant.

Results

The current study included 40 eyes of 42 patients with NFPA and 40 eyes of 40 healthy controls. Among these samples, four eyes of two patients with low QI, age-related macular degeneration, macular drusen, or epiretinal membrane were excluded. There were no significant differences in age, sex, SE, IOP, or QI of 4.5-mm × 4.5-mm HD disc scanning or 6-mm × 6-mm HD retina scanning. The BCVA ($P = 0.003$) and VF metrics ($P < 0.001$) of the NFPA group were significantly worse than those of the control group. Visual acuity impairments occurred in five patients with NFPA secondary to serous visual field defects affecting central vision. More data and information about these eyes are presented in Supplementary Table S1.

Table 1. Demographic and Clinical Information of the NFPA Group and Control Group

Characteristic	NFPA	Control	*P* Value
Age, y	45.13 (13.25)	45.33 (13.38)	0.947[a]
Sex, male/female	20/20	20/20	
IOP, mm Hg	15.21 (2.61)	14.83 (2.36)	0.500[a]
SE, D	−1.36 (2.02)	−1.14 (2.30)	0.456[b]
BCVA, logMAR	0.08 (0.26)	−0.02 (0.05)	**0.018**[b]
MD, dB	8.03 (7.80)	0.29 (0.98)	**<0.001**[b]
MS, dB	19.85 (8.15)	28.22 (1.17)	**<0.001**[a]
QI, HD disc 4.5 × 4.5 mm	8.61 (0.67)	8.67 (0.79)	0.659[b]
QI, HD retina 6 × 6 mm	7.87 (0.87)	8.00 (0.75)	0.743[b]
mGCC average, µm	93.55 (12.77)	99.35 (5.26)	**0.010**[a]
mGCC superior, µm	93.27 (13.20)	98.89 (5.24)	**0.015**[a]
mGCC inferior, µm	93.85 (12.74)	99.83 (5.72)	**0.008**[a]
mGCC FLV, %	2.83 (3.98)	0.43 (0.33)	**<0.001**[b]
mGCC GLV, %	6.52 (9.56)	1.52 (1.90)	**0.001**[b]
pRNFL average, µm	96.55 (17.25)	105.79 (7.42)	**0.003**[a]
pRNFL NU, µm	71.60 (17.07)	81.84 (15.00)	**0.031**[b]
pRNFL NL, µm	65.79 (15.91)	75.97 (12.24)	**0.002**[a]
pRNFL IN, µm	106.96 (23.84)	111.93 (14.50)	0.264[a]
pRNFL IT, µm	136.06 (25.34)	149.23 (17.75)	**0.009**[a]
pRNFL TL, µm	61.39 (12.52)	73.24 (10.11)	**<0.001**[a]
pRNFL TU, µm	78.02 (17.43)	88.89 (15.47)	**0.012**[b]
pRNFL ST, µm	139.39 (26.50)	141.03 (25.03)	0.777[a]
pRNFL SN, µm	113.18 (26.22)	117.53 (22.45)	0.428[a]
FAZ area, mm^2	0.36 (0.11)	0.29 (0.08)	**0.002**[b]
FAZ perimeter, mm	2.32 (0.38)	2.06 (0.31)	**0.003**[b]
Duration, y	1.21 (1.85)		
Coronal SSE, cm	1.41 (0.84)		
Sagittal SSE, cm	1.05 (0.57)		
Chief complaints, %			
Headache	19.7		
Visual impairment	22.4		
No symptoms	46.1		
NA	11.8		

Values are presented as mean (SD) unless otherwise indicated. The measured area of pRNFL was evenly divided into eight subsectors: nasal-upper (NU), nasal-lower (NL), inferior-nasal (IN), inferior-temporal (IT), temporo-lower (TL), temporo-upper (TU), superior-temporal (ST), and superior-nasal (SN) sectors. FLV, focal loss of volume; GLV, general loss of volume; logMAR, logarithm of the minimum angle of resolution; MS, mean sensitivity of perimetry; NA, not available.

[a]Independent samples *t*-test.

[b]Mann-Whitney *U* test.

The mean duration from the onset of symptoms to the diagnosis of NFPA was 1.21 years, ranging from 0.01 to 7.8 years. The optic chiasms of all patients were compressed to varying degrees, except for three participants. The mean coronal and sagittal SSEs were 1.41 ± 0.84 cm and 1.05 ± 0.57 cm, respectively. Regarding the chief complaints, most patients (46.1%) had no symptoms, and the suspected lesion was mostly found by routine physical examination. A total of 22.4% and 19.7% of patients presented with visual impairments or headache, respectively (Table 1).

The parameters related to the pRNFL and GCC are also listed in Table 1. Compared to those in the control group, all GCC metrics were significantly decreased in the NFPA group (all $P \leq 0.05$). The pRNFL thickness of most sectors was also obviously thinner in patients

Table 2. Comparison of the Vessel Density Between the NFPA Group and Control Group

Vessel Density	NFPA, Mean (SD), %	Control, Mean (SD), %	*P* Value
SCP whole image	49.09 (3.13)	49.25 (2.83)	0.936[a]
SCP parafoveal average	51.67 (3.40)	51.67 (3.61)	0.996[b]
SCP temporal	51.90 (3.60)	51.28 (3.80)	0.459[b]
SCP superior	52.26 (3.98)	52.38 (3.86)	0.892[b]
SCP nasal	50.67 (4.42)	50.75 (4.23)	0.930[b]
SCP inferior	51.84 (3.68)	52.27 (3.74)	0.606[b]
SCP perifoveal average	49.88 (3.45)	50.02 (3.01)	0.988[a]
SCP temporal	46.59 (3.22)	45.78 (3.69)	0.307[b]
SCP superior	50.03 (4.01)	50.27 (2.94)	0.830[a]
SCP nasal	53.00 (3.66)	53.98 (3.17)	0.210[b]
SCP inferior	49.91 (3.84)	50.11 (3.27)	0.808[b]
DCP whole image	50.32 (4.97)	47.65 (5.10)	**0.011**[a]
DCP parafoveal average	55.83 (3.71)	54.35 (4.04)	**0.022**[b]
DCP temporal	56.48 (3.74)	55.17 (3.77)	0.127[b]
DCP superior	55.60 (4.49)	53.55 (4.67)	0.052[b]
DCP nasal	56.42 (3.78)	55.38 (3.92)	0.240[b]
DCP inferior	54.83 (4.06)	53.29 (4.73)	0.128[b]
DCP perifoveal average	51.63 (5.48)	48.53 (5.68)	**0.017**[b]
DCP temporal	54.69 (4.16)	52.73 (5.12)	0.068[b]
DCP superior	51.31 (6.03)	47.77 (6.37)	**0.007**[a]
DCP nasal	50.47 (6.37)	46.82 (5.92)	**0.011**[b]
DCP inferior	49.99 (6.53)	46.74 (6.82)	**0.035**[b]
RPC whole image	48.38 (4.56)	50.71 (1.88)	**0.010**[a]
RPC peripapillary average	50.08 (6.13)	53.47 (2.41)	**0.002**[b]
RPC NS	46.16 (7.85)	49.61 (2.64)	**0.010**[b]
RPC NI	44.42 (7.64)	47.64 (3.99)	**0.021**[b]
RPC IN	50.09 (7.02)	52.72 (3.40)	**0.036**[b]
RPC IT	56.75 (6.12)	58.95 (3.51)	0.052[b]
RPC TI	49.95 (6.35)	56.27 (3.98)	**0.000**[b]
RPC TS	53.89 (6.24)	56.92 (4.09)	**0.013**[b]
RPC ST	54.96 (7.86)	57.53 (3.92)	0.303[a]
RPC SN	48.29 (7.42)	51.50 (4.49)	**0.023**[b]

The measured area of angio retina scan centered on the fovea was divided into four quadrants according to the ETDRS grid. The measured area of the angio disc scan was automatically divided based on the Garway Heath method into eight subsectors: nasal-superior (NS), nasal-inferior (NI), inferior-nasal (IN), inferior-temporal (IT), temporo-inferior (TI), temporo-superior (TS), superior-temporal (ST), and superior-nasal (SN) sectors.

[a]Mann-Whitney *U* test.

[b]Independent samples *t*-test.

than in healthy control individuals (all $P < 0.03$), except for that of the SN, ST, and IN sectors. The FAZ area ($P = 0.002$) and perimeter ($P = 0.003$) of patients with NFPA were much larger than those of healthy controls.

Comparisons of microvascular densities were conducted among different sectors of the parafoveal and perifoveal areas (Table 2). No significant differences were found in VD at the SCP segment. In most sectors of the perifoveal area, the VDs of the DCP segment were significantly increased (all $P < 0.05$) in the NFPA group compared to those in the controls, except for the temporal sector ($P = 0.068$). To confirm the differences in macular VD mentioned before, multivariable regression analyses were conducted (Table 3). After adjusting for age, sex, SE, and QI, most results presented no alterations (all $P < 0.05$), except for VD at the temporal sector of the perifoveal area ($P = 0.024$).

Table 3. Multivariable Analyses of Vessel Density Between the NFPA Group and Control Group

Vessel Density	Estimate	95% Confidence Interval	*P* Value
RPC whole image	−1.60	−3.00 to −0.19	**0.027**
RPC peripapillary	−2.73	−4.66 to −0.79	**0.007**
RPC NS	−2.69	−5.24 to −0.15	**0.038**
RPC NI	−3.02	−5.82 to −0.23	**0.034**
RPC IN	−1.50	−3.75 to 0.75	0.186
RPC IT	−0.894	−3.04 to 1.25	0.408
RPC TI	−6.95	−9.32 to −4.58	**<0.001**
RPC TS	−2.913	−5.49 to −0.33	**0.028**
RPC ST	−1.44	−4.14 to 1.26	0.289
RPC SN	−1.65	−4.61 to 1.31	0.269
SCP whole image	0.23	−0.99 to 1.44	0.709
SCP parafoveal average	0.34	−1.35 to 2.03	0.689
SCP perifoveal average	0.33	−0.93 to 1.60	0.601
DCP whole image	3.17	1.08 to 5.25	**0.004**
DCP parafoveal average	2.07	0.40 to 3.74	**0.016**
DCP perifoveal average	3.56	1.22 to 5.89	**0.003**
DCP temporal	2.26	0.31 to 4.22	**0.024**
DCP superior	3.69	0.99 to 6.41	**0.008**
DCP nasal	4.39	1.63 to 7.16	**0.002**
DCP inferior	3.85	1.03 to 6.66	**0.008**
FAZ area, mm^2	0.08	0.03 to 0.13	**0.002**
FAZ perimeter, mm	0.28	0.11 to 0.46	**0.002**

The measured area of the angio disc scan was automatically divided based on the Garway Heath method into eight subsectors: nasal-superior (NS), nasal-inferior (NI), inferior-nasal (IN), inferior-temporal (IT), temporo-inferior (TI), temporo-superior (TS), superior-temporal (ST), and superior-nasal (SN) sectors. The measured area of angio retina scan was divided into four quadrants according to the ETDRS grid.

Multivariable linear regression analyses were conducted after adjusting for age, sex, spherical equivalent, and image quality to compare vessel densities between patients and healthy controls.

Capillary density centered on the optic disc of patients with NFPA obviously decreased in the whole image and in the peripapillary area analyzed by independent samples *t*-test (all $P < 0.01$) (Table 2). The results also showed diffuse attenuation of VD in the RPC segment among different sectors in patients (all $P < 0.05$), except for the ST sector ($P = 0.303$). After adjusting for age, sex, SE, and QI, we found that the difference in VD of the RPC segment at the IN, IT, ST, and SN sectors became insignificant between the NFPA group and the control group (Table 3).

To explore the relationships between VD and visual function, retinal structure, and tumor size, multivariable regression analyses were conducted in affected eyes after adjusting for age, sex, SE, and QI (Table 4). The results revealed that microvascular densities in the RPC segment in the peripapillary area were significantly related to MD, pRNFL, and macular GCC (mGCC) thickness. Peripapillary VD was also negatively associated with coronal and sagittal SSE before or after controlling visual function and retinal structure (all $P \leq 0.01$). For every 1 mm of coronal SSE, the VD in the RPC segment in the peripapillary area decreased by approximately 4%. For macular metrics, the perifoveal and parafoveal VDs in the DCP segment were positively correlated with MD (all $P \leq 0.022$). Microcirculation in the DCP segment in the parafoveal area was negatively related to pRNFL and mGCC thickness (all $P \leq 0.021$). The associations between microvascular density in the DCP segment and tumor size were also significant, but this result became insignificant after controlling visual function and retinal structure.

The ROC curves of significant measurements that indicate diagnostic performance are shown in Figure 2. We found that the AUCs of MD (0.892; 95% confidence interval [CI], 0.81–0.97; $P < 0.001$) and RPC in the TI sector (0.801; 95% CI, 0.70–0.90; $P < 0.001$)

Table 4. The Association Between Vessel Density and Visual Function, Retinal Structure, and Tumor Size

	Parafoveal DCP		Perifoveal DCP		Peripapillary RPC	
Vessel Density	Estimate (95% CI)	*P* Value	Estimate (95% CI)	*P* Value	Estimate (95% CI)	*P* Value
Model 1						
BCVA	1.38 (−4.25, 7.00)	0.613	3.39 (−3.87, 10.64)	0.338	0.80 (−8.17, 9.77)	0.853
MD	0.25 (0.07, 0.43)	**0.009**	0.30 (0.05, 0.54)	**0.022**	−0.35 (−0.64, −0.06)	**0.022**
pRNFL	−0.13 (−0.23, −0.03)	**0.012**	−0.11 (−0.25, 0.04)	0.141	0.33 (0.23, 0.44)	**<0.001**
mGCC	−0.15 (−0.27, −0.03)	**0.021**	−0.15 (−0.32, 0.02)	0.086	0.32 (0.14, 0.50)	**0.002**
Model 2						
Coronal SSE	2.24 (0.76, 3.72)	**0.006**	2.21 (0.03, 4.39)	**0.048**	−4.27 (−6.33, −2.20)	**0.001**
Sagittal SSE	2.68 (−0.01, 5.37)	**0.05**	2.16 (−1.59, 5.90)	0.233	−5.33 (−8.50, −2.17)	**0.003**
Model 3						
Coronal SSE	0.92 (−2.45, 4.29)	0.562	0.17 (−4.87, 5.22)	0.941	−4.15 (−7.13,−1.17)	**0.010**
Sagittal SSE	−1.57 (−6.86, 3.72)	0.523	−4.77 (−11.70, 2.17)	0.157	−3.22 (−8.70, 2.25)	0.219

Multivariable regression analyses of models 1 and 2 were conducted after adjusting for age, sex, spherical equivalent, and image quality. Multivariable regression analyses of model 3 were conducted after adjusting for age, sex, spherical equivalent, image quality, MD, and the corresponding retinal structure (pRNFL or mGCC). The parameters of visual function (BCVA and MD), retinal structure (pRNFL and mGCC), and tumor size (coronal and sagittal SSE) were all continuous variables.

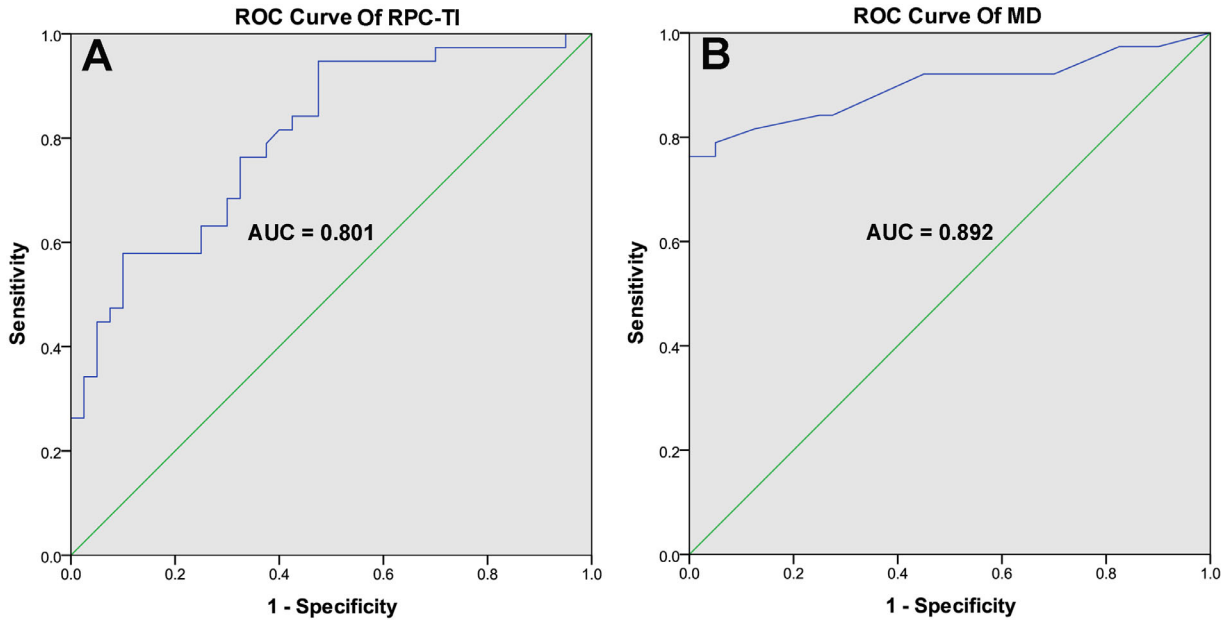

Figure 2. ROC curves between patients with NFPA and healthy controls. (A) The ROC curves of RPC-TI. (B) The ROC curves of MD. RPC-TI, vessel density in the radial peripapillary capillary segment of the temporal-inferior sector.

were the largest. The cutoff value of VD in the RPC segment in the TI sector was 52.05%, with 59% sensitivity and 90% specificity (Table 5).

Discussion

To the best of our knowledge, this study provided a basis for an improved understanding of the relationship between the sellar local mass effect and fundus structures and VD changes without abnormal hormone secretion. The most remarkable results of our research were that patients with NFPA had a larger FAZ area and perimeter, thinner GCC and pRNFL thickness, lower VD in the RPC segment of the peripapillary area, and higher VD in the DCP segment than healthy participants. The correlations between fundus microvascular densities and VFD or

Table 5. ROC Curves Between Patients With NFPA and Healthy Controls

Characteristic	AUC	95% CI	*P* Value	Cutoff	Sensitivity	Specificity
MD	**0.892**	(0.81, 0.97)	**<0.001**	2.15 dB	0.75	1
BCVA	0.625	(0.50, 0.75)	**0.06**	−0.04	0.86	0.35
mGCC average	0.626	(0.50, 0.75)	**0.06**	95.36 µm	0.50	0.85
pRNFL average	0.639	(0.52, 0.76)	**0.03**	94.57 µm	0.34	0.98
RPC average	0.664	(0.54, 0.78)	**0.01**	49.10%	0.32	0.98
RPC NS	0.583	(0.45, 0.71)	0.21	44.62%	0.39	0.97
RPC NI	0.595	(0.47, 0.72)	0.15	42.66%	0.37	0.90
RPC TS	0.643	(0.52, 0.77)	**0.03**	57.50%	0.79	0.53
RPC TI	**0.801**	(0.70, 0.90)	**<0.001**	52.05%	0.59	0.90
DCP-parafoveal average	0.619	(0.49, 0.75)	**0.07**	53.40%	0.78	0.48
DCP-perifoveal average	0.676	(0.55, 0.80)	**0.01**	48.15%	0.75	0.60
DCP-perifoveal-T	0.608	(0.48, 0.74)	0.11	49.38%	0.92	0.33
DCP-perifoveal-S	0.692	(0.57, 0.81)	**<0.001**	47.44%	0.83	0.60
DCP-perifoveal-N	0.680	(0.56, 0.80)	**0.01**	53.71%	0.42	0.90
DCP-perifoveal-I	0.646	(0.52, 0.77)	**0.03**	48.79%	0.61	0.70
FAZ area	0.702	(0.58, 0.82)	**<0.001**	0.32 mm^2	0.64	0.73
FAZ perimeter	0.695	(0.58, 0.81)	**<0.001**	2.28 mm	0.53	0.83

The measured area of the pRNFL was automatically and evenly divided into eight subsectors: nasal-upper (NU), nasal-lower (NL), inferior-nasal (IN), inferior-temporal (IT), temporo-lower (TL), temporo-upper (TU), superior-temporal (ST), and superior-nasal (SN) sectors. The measured area of the angio disc scan was automatically divided based on the Garway Heath method into eight subsectors: nasal-superior (NS), nasal-inferior (NI), inferior-nasal (IN), inferior-temporal (IT), temporo-inferior (TI), temporo-superior (TS), superior-temporal (ST), and superior-nasal (SN) sectors. The measured area of angio retina scan was divided into four quadrants according to the ETDRS grid.

retinal structure were significant. Peripapillary VD in the RPC segment was significantly and negatively related to sellar mass size.

In accordance with previous results concerning OCTA evaluation of PAs, we confirmed the morphologic structural changes of the retina caused by NFPA. According to our results, the pRNFL thickness of patients presented as a diffuse decrease with a more serious reduction in horizontal sectors. For GCC thickness, the reduction in average, superior half, and inferior half thickness in the NFPA group was also shown in our study. Retrograde degeneration of RGC axons with long-standing chiasmal compression is the most likely mechanism for the change in thickness measurements.[13,14] The characteristic pRNFL defects may be attributed to the particular pathway by which RGC axons enter the optic disc. Sella region masses predominantly exhibit damage on crossing nerve fibers originating from the nasal hemiretina, and the horizontal sectors of the optic disc receive RGC axons from cells located in the nasal half of the macula and nasal retina to the optic disc.[15] Additionally, enlargement of the FAZ area and perimeter of patients with NFPA was observed in our study. Histologically, the FAZ border is a single-layered capillary arcade located in the ganglion cell layer, and its sensitivity to ischemia and oxygen supply has been shown in several diseases, such as retinal vein occlusion and diabetic retinopathy.[16,17] The FAZ area was also significantly related to VF loss.[18]

With the advent of OCTA, fundus microcirculation could be quantitively and noninvasively visualized and analyzed. Consistent with the results of previous studies,[7,10] our results also demonstrated that patients exhibited a decreased microvascular density in the RPC segment in the peripapillary area, with a more serious reduction in the temporal and nasal sectors, which was similar to the characteristic pattern of pRNFL thickness changes.[19,20] Nonetheless, unlike earlier studies in which different types of PA or sellar mass lesions were pooled together, the present study only detected microvascular alterations of the fundus in patients with NFPA. The results revealed that VD in the SCP segment was not significantly different between patients and healthy controls. In contrast, except for VD of the temporal sector, which adhered to the preferential ganglion cell loss in the nasal hemiretina caused by PA, VD in the DCP segment of the perifoveal area was much greater in patients with NFPA than in controls.[21,22] It has been well established that because of their unusually high energy and

metabolism demands, RGCs are sensitive to the supply of energy sources (oxygen and other substrates).[6,23] Pertinently, the regional vascular network is vitally important to sustain such high requirements. In terms of our study, since enrolled patients had mild VFDs, we possibly conducted a cross-sectional study at a relatively early stage of disease. Although peripapillary VD obviously decreased, macular VD in the SCP segment only indicated mild damage without a significant difference, whereas the blood flow in the DCP segment was compensatorily enhanced. It may also hint that OCTA scanning was more sensitive than VF tests to reflect the micro-alterations of the posterior pole caused by NFPA. To confirm this speculation, additional research efforts are required. Since the influence of NFPA on the two eyes could be discrepant, our study further enrolled both eyes of study participants to explore these changes in visual function, retinal structure, and microcirculation in patients with NFPA by multilevel regression analysis (Supplementary Tables S2 and S3).

Our study also substantiated that VFD, retinal structure loss, or tumor size was significantly associated with VD in the peripapillary area or in the DCP segment (Table 4). The decreasing VD is correlated with larger tumor size or worse impairment of retinal structure and VFD. After adjusting visual function and retinal structure, the mass size was only significantly related to VD in the RPC segment in the peripapillary area. This result might be explained by the fact that a larger mass can cause more serious chiasmal compression and axonal retrograde degeneration,[24] resulting in more severe microvascular damage in the peripapillary area. However, the possibility that NFPA can directly damage the fundus microcirculation cannot be excluded in the present study, and further study is needed to explore the microvascular density of patients with NFPA before VF loss and structural thickness damage.

In the present study, the diagnostic performance among different parameters was also evaluated, including visual function (MD and BCVA), retinal structure (pRNFL and mGCC), and VD metrics. The AUC of the VD at the TI subsector in the RPC segment was similar to that of MD, which was much larger than that of BCVA and other structural parameters. It is possible that in clinical practice, both the measurement of visual field and microvascular density of fundus could assist in the diagnosis of NFPA.

Admittedly, several limitations of the current study should be taken into consideration. (1) As a retrospective cross-sectional study, the present study cannot observe alterations in VD along with disease progression. (2) Due to the lack of patients' axial length information, our analyses adjusted SE, age, sex, and QI. (3) All data were derived from a single center, and all participants were Asian. (4) The mechanism of retinal microcirculation alterations caused by anatomical variation in NFPA has not been elucidated. Consequently, several large-scale, multicentric, prospective, and high-quality studies are still required to illustrate the microvascular changes of patients with NFPA at different stages of disease, which could further confirm the correlation among mass size, disease duration, and fundus VD and could even support an exploration of the underlying mechanism of the mass effect on VD changes.

In summary, in this cross-sectional study, the retinal microvascular impairments of patients with NFPA presented as obviously decreased VD in the RPC segment of the horizonal sectors of the peripapillary area and significantly increased blood flow in the DCP segment of the perifoveal area. Moreover, the peripapillary microvascular densities of patients were significantly associated with sellar mass size. VD in the RPC segment in the TI sector provides information that may assist clinicians in the diagnosis of NFPA.

Acknowledgments

The authors thank Ye Wang, who works at Department of Epidemiology and Statistics, Institute of Basic Medical Sciences, Chinese Academy of Medical Sciences, School of Basic Medicine, Peking Union Medical College, Beijing, China, for statistical advice.

Disclosure: **X. Wang**, None; **Y. Chou**, None; **H. Zhu**, None; **B. Xing**, None; **Y. Yao**, None; **L. Lu**, None; **H. You**, None; **L. Gan**, None; **M. Wang**, None; **J. Ma**, None; **Y. Zhong**, None

[*] XW and YC contributed equally to this work.

References

1. Ntali G, Wass JA. Epidemiology, clinical presentation and diagnosis of non-functioning pituitary adenomas. *Pituitary*. 2018;21(2):111–118.
2. Yona G, Naftali S. Non-functioning pituitary adenomas. *Best PRACTt Res Clin Endocrinol Metab.* 2009;23(5):625–638.
3. Ferrante E, Ferraroni M, Castrignano T, et al. Non-functioning pituitary adenoma database: a useful resource to improve the clinical

management of pituitary tumors. *Eur J Endocrinol*. 2006;155(6):823–829.
4. Di Somma C, Scarano E, de Alteriis G, et al. Is there any gender difference in epidemiology, clinical presentation and co-morbidities of non-functioning pituitary adenomas? A prospective survey of a national referral center and review of the literature. *J Endocrinol Invest.* 2021;44(5):957–968.
5. Rogers A, Karavitaki N, Wass JA. Diagnosis and management of prolactinomas and non-functioning pituitary adenomas. *BMJ*. 2014;349:g5390.
6. Yu DY, Cringle SJ, Balaratnasingam C, Morgan WH, Yu PK, Su EN. Retinal ganglion cells: energetics, compartmentation, axonal transport, cytoskeletons and vulnerability. *Prog Retin Eye Res*. 2013;36:217–246.
7. Lee GI, Park KA, Oh SY, Kong DS. Analysis of optic chiasmal compression caused by brain tumors using optical coherence tomography angiography. *Sci Rep.* 2020;10(1):2088.
8. Dallorto L, Lavia C, Jeannerot AL, et al. Retinal microvasculature in pituitary adenoma patients: is optical coherence tomography angiography useful?. *Acta Ophthalmol*. 2020;98(5):e585–e592.
9. Lee GI, Park KA, Oh SY, Kong DS. Parafoveal and peripapillary perfusion predict visual field recovery in chiasmal compression due to pituitary tumors. *J Clin Med*. 2020;9(3):697.
10. Cennamo G, Solari D, Montorio D, et al. Early vascular modifications after endoscopic endonasal pituitary surgery: the role of oct-angiography. *PLoS One*. 2020;15(10):e241295.
11. Sarkar S, Philip VJ, Cherukuri SK, Chacko AG, Chacko G. Implications of the world health organization definition of atypia on surgically treated functional and non-functional pituitary adenomas. *Acta Neurochir (Wien)*. 2017;159(11):2179–2186.
12. Gan L, Ma J, Feng F, et al. The predictive value of suprasellar extension for visual function evaluation in Chinese patients with nonfunctioning pituitary adenoma with optic chiasm compression. *World Neurosurg*. 2018;116:e960–e967.
13. Moon CH, Hwang SC, Kim BT, Ohn YH, Park TK. Visual prognostic value of optical coherence tomography and photopic negative response in chiasmal compression. *Invest Ophthalmol Vis Sci.* 2011;52(11):8527–8533.
14. Keller J, Sánchez-Dalmau BF, Villoslada P. Lesions in the posterior visual pathway promote trans-synaptic degeneration of retinal ganglion cells. *PLoS One*. 2014;9(5):e97444.
15. Al-Louzi O, Prasad S, Mallery RM. Utility of optical coherence tomography in the evaluation of sellar and parasellar mass lesions. *Curr Opin Endocrinol Diabetes Obes.* 2018;25(4):274–284.
16. Wons J, Pfau M, Wirth MA, Freiberg FJ, Becker MD, Michels S. Optical coherence tomography angiography of the foveal avascular zone in retinal vein occlusion. *Ophthalmologica*. 2016;235(4):195–202.
17. Ragkousis A, Kozobolis V, Kabanarou S, et al. Vessel density around foveal avascular zone as a potential imaging biomarker for detecting preclinical diabetic retinopathy: an optical coherence tomography angiography study. *Semin Ophthalmol*. 2020;35(5–6):316–323.
18. Kwon J, Choi J, Shin JW, Lee J, Kook MS. Alterations of the foveal avascular zone measured by optical coherence tomography angiography in glaucoma patients with central visual field defects. *Invest Ophthalmol Vis Sci*. 2017;58(3):1637–1645.
19. Ana B, Cristina S, Ioan Stefan F. Optical coherence tomography impacts the evaluation of visual pathway tumors. *Neurosurg Rev*. 2018;41(2):415–426.
20. Monteiro MLR, Leal BC, Rosa AAM, Bronstein MD. Optical coherence tomography analysis of axonal loss in band atrophy of the optic nerve. *Br J Ophthalmol.* 2004;88(7):896–899.
21. Blanch RJ, Micieli JA, Oyesiku NM, Newman NJ, Biousse V. Optical coherence tomography retinal ganglion cell complex analysis for the detection of early chiasmal compression. *Pituitary*. 2018;21(5):515–523.
22. Jeong AR, Kim EY, Kim NR. Preferential ganglion cell loss in the nasal hemiretina in patients with pituitary tumor. *J Neuroophthalmol*. 2016;36(2):152–155.
23. Yu DY, Cringle SJ. Oxygen distribution and consumption within the retina in vascularised and avascular retinas and in animal models of retinal disease. *Prog Retin Eye Res*. 2001;20(2):175–208.
24. Zhang Y, Ye Z, Wang M, Qiao N. Ganglion cell complex loss precedes retinal nerve fiber layer thinning in patients with pituitary adenoma. *J Clin Neurosci*. 2017;43:274–277.